

Circuit modeling and analysis of matching configurations for the DTT ICRF system

*Original*

Circuit modeling and analysis of matching configurations for the DTT ICRF system / Cioffi, Alfredo; Ceccuzzi, Silvio; Milanesio, Daniele; Ponti, Cristina; Ravera, Gian Luca; Schettini, Giuseppe. - In: EPJ WEB OF CONFERENCES. - ISSN 2100-014X. - ELETTRONICO. - 346:(2026). ( 25th Topical Conference on Radio-Frequency Power in Plasmas (RFPPC2025) Schloss Hohenkammer (Ger) May 19-22, 2025) [10.1051/epjconf/202634603006].

*Availability:*

This version is available at: 11583/3006643 since: 2026-01-16T11:10:00Z

*Publisher:*

EDP Sciences

*Published*

DOI:10.1051/epjconf/202634603006

*Terms of use:*

This article is made available under terms and conditions as specified in the corresponding bibliographic description in the repository

*Publisher copyright*

(Article begins on next page)

# Circuit modeling and analysis of matching configurations for the DTT ICRF system

Alfredo Cioffi<sup>1,3,\*</sup>, Silvio Ceccuzzi<sup>1,2</sup>, Daniele Milanesio<sup>4</sup>, Cristina Ponti<sup>3</sup>, Gian Luca Ravera<sup>2</sup>, and Giuseppe Schettini<sup>3</sup>

<sup>1</sup>DTT S.C. a r.l., Via Enrico Fermi 45, 00044, Frascati, Italy

<sup>2</sup>ENEA, Nuclear Dept., Via Enrico Fermi 45, 00044, Frascati, Italy

<sup>3</sup>Università degli Studi Roma Tre, DIEM, Via Vito Volterra 62, 00146, Rome, Italy

<sup>4</sup>Politecnico di Torino, DET, Corso Duca degli Abruzzi 24, 10129 Turin, Italy

**Abstract.** In Ion Cyclotron Range of Frequencies (ICRF) systems, transmission lines, based on rigid coaxial cables, deliver the power from the radiofrequency generators to the antennas, matching the impedances to protect the generator, and maximizing the power transfer to the plasma. This work performs such an analysis, employing a circuitual approach to evaluate different matching configurations, checking the maximum voltage all over the cables and avoiding heavy electromagnetic simulation for a quick and easy comparison. Simulations were run for the ICRF system of the Divertor Tokamak Test facility (DTT) using the circuit simulation tool of Ansys Electronic Desktop. After choosing which circuit fits the best in this application, the whole antenna matching circuit was modelled and verified through the active S-parameters. The analysis has proceeded by drawing the ELM resilient schemes for two antennas with -3dB hybrid couplers, showing the power reflected into the dummy load varying the power ratio and the phasing between the straps by a source tapering of amplitude and phase at the generator.

## 1 Introduction

Radiofrequency (RF) systems at the Ion Cyclotron Resonant Frequencies (ICRF) are one of the main additional heating tools in tokamaks and other fusion devices due to their consolidated technology and effective uses also beyond heating. ICRF systems are profitably used in most existing fusion devices like AUG, EAST, WEST, W7-X and their installation is planned in future machines like CFETR, ITER, and SPARC. An ICRF system is also foreseen in the Divertor Tokamak Test facility (DTT) [1], a new tokamak under realization at the ENEA Frascati Research Center with main parameters:  $B_0 = 6$  T,  $I_p = 5.5$  MA,  $R_0 = 2.19$  m,  $a = 0.7$  m, and pulse length around 100 s. DTT aims at studying divertor solutions able to cope with the power exhaust and the thermal load in a relevant scenario for DEMO future tokamak, with a flexibility in terms of magnetic configurations. Therefore delivering a large amount of power to the plasma will be a key element. Depending on the achievements or issues with the first installations, the ICRF system may consist of two, four or six antennas [2]. DTT ICRF system project is meant to work in a large frequency range from 60 to 90 MHz and designed to deliver 3 MW to the plasma through a pair of 3-strap antennas.

A careful analysis of the matching network in ICRF systems is of paramount importance to avoid dead bands in the operational frequency range and optimize the number

of expensive components to be installed. The matching has three essential goals [3]:

- maximizing the power transfer to the antenna and minimizing the power loss in the feed line;
- controlling the antenna array current spectrum in amplitude and phase as a requirement to the different heating and current drive scenarios;
- avoiding tripping the generator, protecting it against high power reflection, especially during fast change of the load due to ELMs.

To satisfy these goals, the transmission line needs tunable components to match the load to the generator in different conditions, an architecture that allows to vary the phase and amplitude between the straps and another layer of architecture to implement load resilient-matching schemes.

This paper reports the latest progress on the design of the transmission line and matching (TLM) circuit scheme of the DTT ICRF system. Many matching options and ELM-resilient schemes have been studied and tested since the initial ICRF systems. In-vessel capacitors, single, double and triple-stub tuners with and without oil, ferrite tuners or frequency variation are some examples of matching options, whilst among ELM-resilient schemes those based on conjugate-T and 3 dB hybrid coupler can be cited [4, 5]. DTT design guidelines recommend to opt for reliable and well-assessed technological solutions, so a 3 dB hybrid coupler load resilient matching scheme with impedance transformers made of a stub tuner and a phase shifter was initially selected as reference circuit [2]. Fig-

\*E-mail: [alfredo.cioffi@dt-project.it](mailto:alfredo.cioffi@dt-project.it), [alfredo.cioffi@uniroma3.it](mailto:alfredo.cioffi@uniroma3.it)

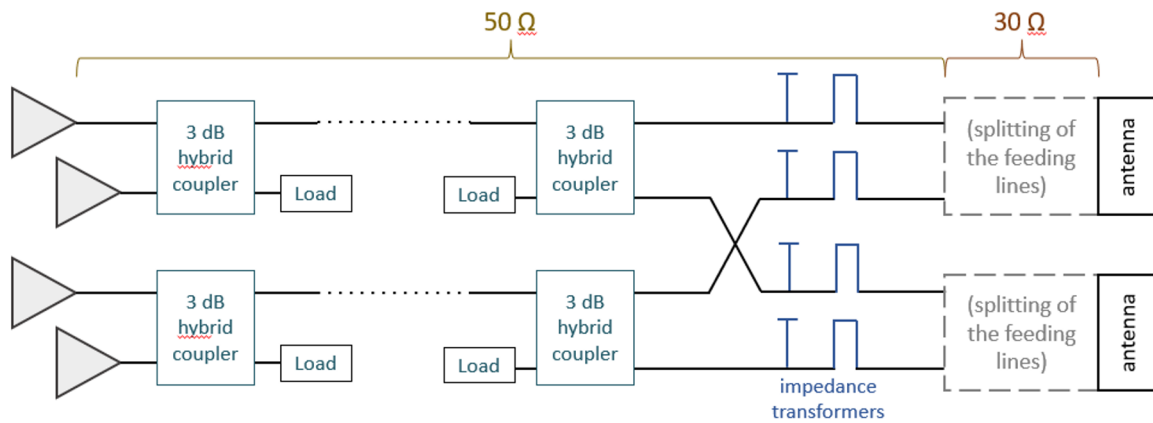


**Figure 1.** Simplified scheme of the ICRF system of DTT.

Figure 1 shows a simplified schematics of such solution that was used as the starting point of this paper analysis aimed at evaluating different matching and pre-matching options.

The paper is organised as follows: in section 2 three more representative circuit alternatives among analysed ones are compared regarding the highest voltage values over all components, separately conducting the simulations of central and side straps. After choosing which circuit fits the best in this application, the whole antenna matching circuit and its performance are presented. In section 3 the analysis proceeds showing the ELM-resilient matching scheme for two antennas. Finally, conclusions are drawn in section 4.

## 2 Antenna matching

### 2.1 Analysis setup

The reference design of the ICRF antenna of DTT is a three-strap coupler with four coaxial feeds, two of which powering an end-fed, centre-grounded, central strap and the other two individually feeding lateral straps. Figure 2 shows the back of the antenna with the position and numbering of the coaxial feeding lines. Owing to strap shape and orientation, to attain an antenna phasing of  $0\pi$ , the following setting is approximately required at the coaxial feeds:

- Top central strap phase (antenna port 1):  $0^\circ$
- Bottom central strap phase (antenna port 2):  $180^\circ$
- Left side strap phase (antenna port 3):  $0^\circ$
- Right side strap phase (antenna port 4):  $0^\circ$

The analysis was conducted in 'Circuit'[6], the circuit simulation tool of Ansys EDT with the T-junction and the antenna modelled by scattering matrices calculated through full-wave electromagnetic simulations. The antenna scattering matrix reproduces to some extent the behaviour of the plasma facing antenna. It was the output of a simulation done with CST Microwave Studio for a dielectric-loaded flat antenna model[7]. Dielectric load

properties were defined to mimic the results of a plasma-loaded antenna simulated with TOPICA considering one of the initial DTT plasma scenarios. When the latter was updated, such dielectric properties were found to underestimate antenna performance by 25%, but circuit analyses keep using them because they result in a conservative approach and allow for a meaningful comparison with the results of past analyses. All circuit components are considered lossless components. The real length of the transmission line, as well as the presence in the circuit of components such as directional couplers, probes, test sections, gas inlet, etc., are not considered in this study due to their low insertion loss and no impact on matching performance.

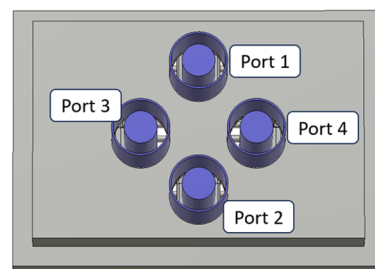


**Figure 2.** Rear view of the flat antenna model, showing the four coaxial ports numbered.

### 2.2 Matching schemes

Investigated circuit alternatives present some common features. The generator is followed by an impedance transformer, then the power is split by a T-junction in two feeding lines that from now on will be referred to as branches. A phase shifter is needed to set the signal phase of a branch with respect to the other branch throughout the frequency range. The following circuit schemes, identified by a letter, were considered:

- *Scheme A*: single stub tuner matching circuit with one trombone per branch

- *Scheme B*: single stub tuner matching circuit, only one branch with the trombone
- *Scheme C*: double stub tuner matching circuit, only one branch with the trombone

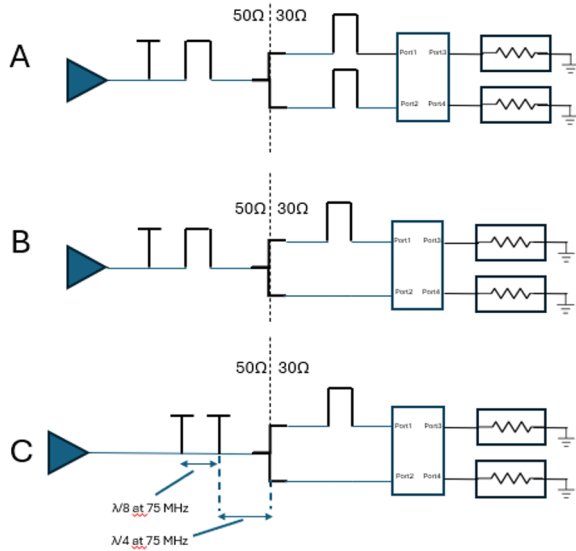


**Figure 3.** RF schemes of principle of the three matching circuits to feed and match the central straps of the DTT ICRF antenna. Port 3 and 4 are terminated on a 50-Ohm grounded resistance.

The circuit schemes of figure 3 are composed by a 30 Ohm characteristic impedance near the antenna, with a transition to 50 Ohm at the T-junction position.

Initially, these matching schemes have been assessed separately on central and outer straps, neglecting the mutual coupling effect, *i.e.* when feeding the central straps from port 1 and 2, the side straps are terminated with a 50-Ohm resistance. Excluding the impedance transformer solution, the major difference between scheme A and B-C is the presence of a phase shifter on both branches. The combination of the phase shifters can be used to set the right phase at the antenna and the voltage anti-node of the standing-wave on the impedance transition at the T-junction over the all range of frequency. Consequently, prioritising the right phase, the maximum of the standing wave at the T-junction was set just at 75 MHz for schemes B and C.

Table 1 summarizes the simulation results for the three schemes and with a total generator output of 1.2 MW (600 kW per strap), corresponding to a source voltage in the simulator  $V_{\text{source}} \approx 11$  kV. In such conditions, the maximum current along the branches lies in the interval [1.27, 1.64] kA. The main results of Table 1 are the maximum voltages, which permit to give an estimate of the power coupling capability (last column). The latter is obtained by scaling the source power by the ratio of the maximum allowable voltage of 35 kV over the maximum voltage,  $V_{\text{MAX}}$ , found along the coaxial lines and compo-

nents through circuit simulations, namely:

$$P_{\text{coupled}} = 1.2 \text{ MW} \cdot (35 \text{ kV})^2 / |V_{\text{MAX}}|^2$$

Since  $S_{11}$  values are very low, *i.e.* the circuit is well matched, such power is also the one that will be coupled to the antenna load.

The results in table 1 show that only scheme A performs reasonably at all frequencies and the same has emerged from lateral straps simulations, not reported here. Several variants of circuit B and C were simulated to check whether it was possible to save one phase shifter from the overall expense of the transmission line. The outcomes are not reported but they are in line with the results of table 1, meaning the importance of having the maximum of the standing wave at the impedance transition point, in order to lower the VSWR.

### 2.3 Performance of a complete antenna

This section shows the results when the circuit schemes for central strap segments and side straps are built into the same simulation. The TLM circuit for the full antenna, choosing the A scheme, is shown in figure 4. In the mechanical model of the antenna, the side straps are connected to the coaxial feeding lines through a metal strip with a width of 120 mm. In the simulations we have accounted for the acquired phase in the strip adding  $-k_0 \cdot 0.12$  m in radians to the side straps generator. This phase delay must be corrected at all frequencies. Therefore simulations were run through the following iterative approach, that following 4 consist in:

1. Fixing the lengths of 'Generator 2' matching components, find the minimum of  $S_{1a}$  varying  $L_{\text{trombone}}$  and  $L_{\text{stub}}$  which are the lengths of 'Generator 1' impedance transformer components
2. Fixing the lengths of 'Generator 1' matching components found at point 1, find the minimum of  $S_{2a}$  varying  $L_{\text{trombone}_2}$  and  $L_{\text{stub}_2}$  which are the lengths of 'Generator 2' impedance transformer components
3. Repeat points 1 and 2 until  $S_{1a}$  and  $S_{2a}$  are reasonably low
4. Check and compensate the phase at the antenna straps, that should be  $[0, \pi, -(k_0 \cdot 0.012 \text{ m}), -(k_0 \cdot 0.012 \text{ m})]$ .
5. Restart from 1.

$S_{1a}$  and  $S_{2a}$  refer to the active scattering parameters of the circuit, *i.e.* the reflection coefficients seen respectively at the ports of the generators 1 and 2 when both are active; the simulation measurement was made thanks to a directional coupler at the generator. Power in the generator is set following the same setup of previous section, *i.e.* 600 kW per strap. Table 2 summarizes the results of the simulation, showing a very low amount of power reflected at the generators. The simulations pointed out that the optimum matching is very sensitive to the length variation of

**Table 1.** Results of the three matching schemes under investigation for the central straps.

Circuit	Frequency [MHz]	Trombone length [mm]	Stub length [mm]	S11 [dB]	Max voltages [kV] for a source power of 1.2 MW					Source power [kW] @35 kV
					stub1	inter-stub link	trombone1 /stub2	branch #1	branch #2	
A	60	1145	245	-33.4	10.9	/	38.1	49.2	49.2	607
	75	957	199	-52.3	10,8	/	37.1	47.9	47.8	641
	90	710	220	-35.4	10.7	/	29.1	37.8	37.8	1029
B	60	2411	51	-21.2	10.9	/	174	48.9	49	49
	75	957	199	-52.3	10,8	/	37.1	47.9	47.8	641
	90	94	1712	-23.9	125.7	/	127.6	38	37.5	90
C	60	1761	2463	-28.8	13.2	10.1	175.5	49	49.3	48
	75	173	1431	-43.7	10.8	35.9	46.5	47.9	47.9	641
	90	1546	197	-28.6	48.2	32.8	30.3	38.2	37.4	633

stub tuners as can be seen from figure 5;  $S_{11}$  and  $S_{1a}$  minima positions are relatively different and a slightly change in the impedance transformer components lengths make their values quickly increase.

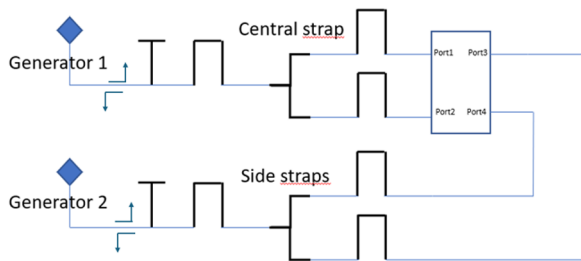


**Figure 4.** RF scheme of principle to feed and match the DTT ICRF antenna

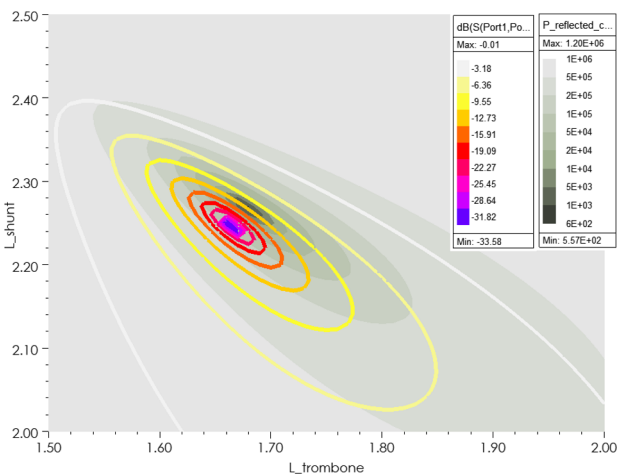


**Figure 5.** Different location of  $S_{11}$  and  $S_{1a}$ , expressed by the power reflected to the central straps generator when both are active, varying the tunable parameters of the impedance transformer of central straps matching circuit. Temperature scale is the  $S_{11}$  whilst the green scale represent  $P_{reflected\_central}$

### 3 ELM resilient schemes

This final section explores ELM-resilient feeding schemes for two antennas, using wideband 3dB hybrid couplers (WHCs). These components are necessary to protect the generator from the reflected power due to the fast load changes during an Edge Localized Mode (ELM), because the tunable matching circuit components cannot be adjusted at the same pace of an ELM. In order to divert the reflected power to the dummy load of the WHC, the waves coming from the feeding lines back to the generator must be in quadrature. In this study an ideal WHC was used.

In figure 6 the ELM resilient matching schemes of the full module of the DTT ICRF system composed by 2 antenna is shown. The first hybrid coupler serves the central straps of both antennas, whilst the second one serves the side straps. If the outgoing transmission lines of each 3 dB hybrid coupler have equal length, the circuit provides ELM resilience.

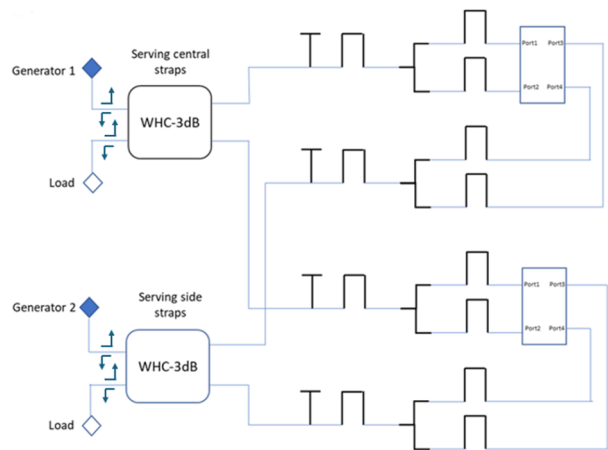


**Figure 6.** RF scheme of principle of the feeding and matching of a module of the DTT ICRH system (2 antennas).

It is worth using this circuit to analyse the effect of the tapering of the source on the generator and antenna sides. From the latter one the interest mostly relies on the electric field component parallel to the DTT magnetic field ( $E_{||}$ ), that is a widely used figure of merit to assess the reduction of RF-induced sputtering [8]. For such analysis a

**Table 2.** Results of the matching circuit of figure 4.

Frequency [MHz]	Straps	Trombone length [mm]	Stub length [mm]	Reflected Power [%]	Stub	Trombone	branch #1	branch #2	Source power [kW] @35 kV
60	central	1681	2261	0.184	37.9	40.0	50.9	50.4	567
	lateral	1700	2240	0.002	34.4	36.0	45.8	46.1	692
75	central	1311	1368	0.012	37.5	38.9	50.0	50.0	588
	lateral	1812	1754	0.022	28.8	30.4	39.1	39.1	962
90	central	1160	1514	0.001	38.8	40.0	50.8	50.8	570
	lateral	1260	1430	0.093	24.9	26.4	32.9	32.9	1358

more accurate model of the antenna was used, importing the scattering matrix returned by TOPICA [9] simulations obtained for the DTT single-null scenario under a flat antenna and plasma slab approximation. The actual antenna geometry will present a double curvature, i.e. over both toroidal and poloidal direction to better match the plasma shape [10], but the flat approximation is widely used for the analysis of antenna  $E_{\parallel}$ . Due to the use of a new scattering matrix, the variable parameters of the matching circuit needed a re-optimisation, which was rather quick because their optimal values were close to those found in the previous section. The coupling between different antennas was neglected so the optimal tuning parameters found for a single antenna can be directly used without re-optimisation in the full circuit of figure 6.

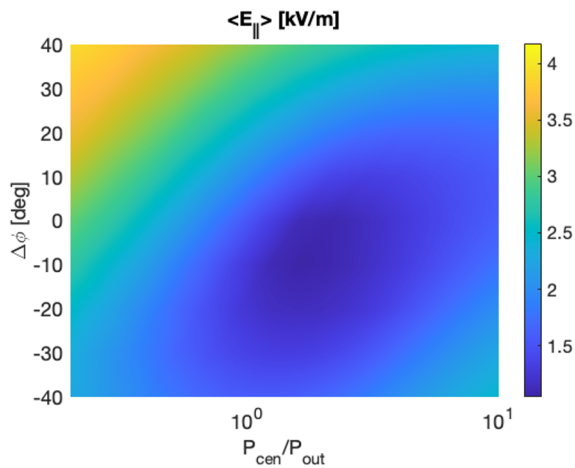


**Figure 7.**  $\langle E_{\parallel} \rangle$  variation sweeping  $P_{\text{central}}/P_{\text{outer}}$  between 0.2 and 10 and  $\Delta\phi$  between  $-40^{\circ}$  and  $40^{\circ}$ . Plot is obtained at  $f = 90$  MHz and  $\langle E_{\parallel} \rangle$  is normalised to fixed coupled power of 1.5 MW.

Calculations have been run in the worst scenario in terms of electric field values, that is, for a frequency of 90 MHz and a strap phasing equal to  $0\pi$ . Parametric studies were carried out versus strap phasing and versus the ratio  $P_{\text{central}}/P_{\text{outer}}$  of the power coupled by the central strap over the power coupled by the lateral straps. Figure 7 depicts the absolute value of the electric field parallel to the DTT magnetic field, averaged at 3mm in front of the right-side limiter,  $\langle E_{\parallel} \rangle$ . A similar analysis has been conducted on the generator side computing the percentage of power diverted toward the dummy load (see figure 8). Comparing the two contour plots, it can be seen that the minima

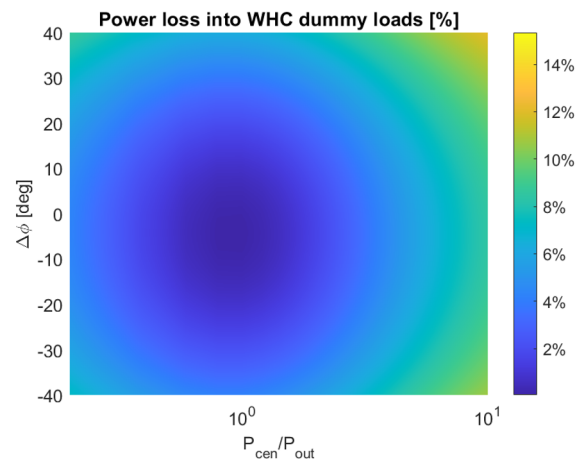


**Figure 8.**  $P_{\text{dummy}}/P_{\text{forward}}$  [%] variation sweeping  $P_{\text{central}}/P_{\text{outer}}$  between 0.2 and 10 and  $\Delta\phi$  between  $-40^{\circ}$  and  $40^{\circ}$ . Plot is obtained at  $f = 90$  MHz.

are in a different working point, meaning that from the operational point of view it will be necessary to find a compromise between lowering the sputtering and minimising lost power.

## 4 Conclusions and future studies

In this study, a circuit simulation framework in ANSYS Circuit tool to easily test different matching options was used to find the best solution for the DTT ICRF system. Single-stub tuner elements with  $Z_0 = 50 \Omega$  solution used to match central or side straps fed by two feeding lines with phase shifter connected with a T-junction properly match DTT ICRF plasma load. Optimization process will be updated with a designed code for multi-optimization objective to make it faster and machine-based. Future studies will assess the effect of ELMs on the circuit with two antennas and whether a decoupling circuit is needed or not.

## References

- [1] F. Romanelli, et al., Divertor Tokamak Test facility project: status of design and implementation, Nuclear Fusion **64**, 112015 (2024). <http://dx.doi.org/10.1088/1741-4326/ad5740>

- [2] S. Ceccuzzi, B. Baiocchi, A. Cardinali, G. Di Gironimo, G. Granucci, D. Liuzza, D. Mascali, G.S. Mauro, D. Milanese, F. Mirizzi et al., The ICRF antenna of DTT: Design status and perspectives, *AIP Conf. Proc.* **2984**, 030015 (2023). <https://doi.org/10.1063/5.0162417>
- [3] P. Dumortier, A.M. Messiaen, ICRH antenna design and matching, *Fusion Science and Technology* **57**, 230 (2010). <https://doi.org/10.13182/FST10-A9414>
- [4] J.M. Noterdaeme, V. Bobkov, S. Brémond, A. Parisot, I. Monakhov, B. Beaumont, P. Lamalle, F. Durodié, M. Nightingale, Matching to ELMy plasmas in the ICRF domain, *Fusion Engineering and Design* **74**, 191 (2005). <https://doi.org/10.1016/j.fusengdes.2005.06.071>
- [5] M. Graham, M.L. Mayoral, I. Monakhov, J. Ongena, T. Blackman, M.P.S. Nightingale, E. Wooldridge, F. Durodié, A. Argouarch, G. Berger-By et al., Implementation of load resilient ion cyclotron resonant frequency (ICRF) systems to couple high levels of ICRF power to ELMy H-mode plasmas in JET, *Plasma Phys. Control. Fusion* **54**, 074011 (2012). <https://doi.org/10.1088/0741-3335/54/7/074011>
- [6] Ansys electronics, <https://www.ansys.com/products/electronics>
- [7] Cst studio suite, <https://www.3ds.com/products/simulia/cst-studio-suite>
- [8] V. Bobkov, D. Aguiam, R. Bilato, S. Brezinsek, L. Colas, H. Faugel, H. Fuenfgelder, A. Herrmann, J. Jacquot, A. Kallenbach et al., Making ICRF power compatible with a high-Z wall in the ASDEX Upgrade, *Plasma Phys. Control. Fusion* **59**, 11 (2017). <https://doi.org/10.1088/0741-3335/59/1/014022>
- [9] V. Lancellotti, D. Milanese, R. Maggiora, G. Vecchi, V. Kyritysya, TOPICA: an accurate and efficient numerical tool for analysis and design of ICRF antennas, *Nucl. Fusion* **46**, S476 (2006). <https://doi.org/10.1088/0029-5515/46/7/S10>
- [10] G. Camera, F.G. Lanzotti, S. Ceccuzzi, G.D. Gironimo, Preliminary Conceptual Design of the ICRH Antenna for DTT: A Systems Engineering Approach, *IEEE Transactions on Plasma Science* **52**, 1 (2024). <https://doi.org/10.1109/TPS.2024.3369469>